ARTICLE

Selective Mechanism of Inhibitors to Two Bromodomains of BRD4 Revealed by Multiple Replica Molecular Dynamics Simulations and Free Energy Analyses

Meng Li[a], Xinguo Liu[a*], Shaolong Zhang[a], Jiahao Sun[a], Qinggang Zhang[a], Jianzhong Chen[b*]

a. School of Physics and Electronics, Shandong Normal University, Jinan 250358, China
b. School of Science, Shandong Jiaotong University, Jinan 250357, China

(Dated: Received on October 7, 2022; Accepted on November 30, 2022)

Bromodomain-containing protein 4 (BRD4) is critical in cell cycle regulation and has emerged as a potential target for treatment of various cancers. BRD4 contains two bromodomains, namely BD1 and BD2. Research suggests that selectively inhibiting BD1 or BD2 may provide more effective treatment options. Therefore, understanding the selective mechanism of inhibitor binding to BD1 and BD2 is essential for development of high selective inhibitors to BD1 and BD2. Multiple replica molecular dynamics (MRMD) simulations are utilized to investigate the binding selectivity of inhibitors SG3-179, GSK778, and GSK620 for BD1 and BD2. The results show that BD1 has stronger structural flexibility than BD2, moreover BD1 and BD2 exhibit different internal dynamics. The analyses of free energy landscapes reveal significant differences in the conformational distribution of BD1 and BD2. Binding free energy predictions suggest that entropy changes, electrostatic interactions, and van der Waals interactions are key factors in the selective binding of BD1 and BD2 by SG3-179, GSK778, and GSK620. The calculations of the energy contributions of individual residues demonstrate that residues (W81, W374), (P82, P375), (Q85, K378), (V87, V380), (L92, L385), (N93, G386), (L94, L387), (C136, C429), (N140, N433), (K141, P434), (D144, H437) and (I146, V439) corresponding to (BD1, BD2) generate significant energy difference in binding of SG3-179, GSK778, and GSK620 to BD1 and BD2, and they can serve as effective targets for development of high selective inhibitors against BD1 or BD2. The related information may provide significant theoretical guidance for improving the selectivity of inhibitors for BD1 and BD2.

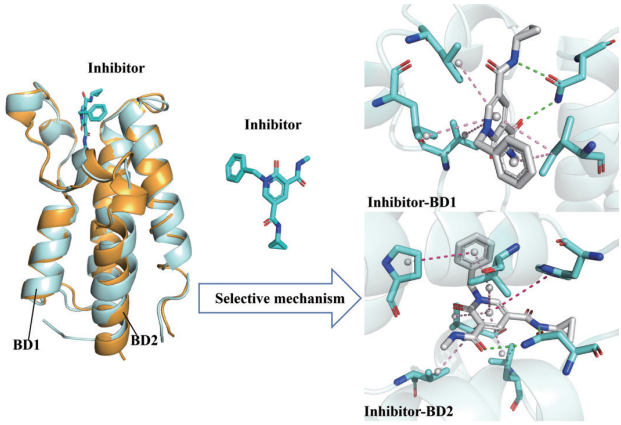

Key words: Bromodomain, Binding selectivity, Multiple replica molecular dynamics simulation, Free energy prediction

I. INTRODUCTION

Bromodomain proteins (BDs) are important epigenetic "readers" that recognize acetylated lysine in histones [1, 2]. BDs play essential roles in regulation of gene transcription, cell cycle control, and chromatin re-

* Authors to whom correspondence should be addressed. E-mail: liuxinguo@sdnu.edu.cn, jzchen@sdjtu.edu.cn

modeling by recruiting transcription factors and chromatin remodeling factors [3–5]. The human proteome encodes 61 BDs from 46 bromodomain-containing proteins (BCPs). All BDs share a common conserved folding structure consisting of four α-helices (αZ, αA, αB, αC), two loops (ZA and BC), and a hydrophobic cavity that recognizes specific sequences of histone ε-N-acetylated lysine residues. BDs are classified into eight subfamilies, and the bromodomain and extra-terminal (BET) family is one of these subfamilies [6]. Bromodomain-containing protein 4 (BRD4) belongs to the BET family, and like other members, contains two sequence-similar BDs (BD1, BD2) and an extra-terminal (ET) structure domain [7]. Related studies have shown that dysfunction of BRD4 may be associated with the emergence of several malignant diseases, like NUT midline cancer, Burkitt's lymphoma, acute myeloid leukemia, and inflammatory diseases [8–11]. Furthermore, several studies have shown that inhibition of the interaction of acetylated lysine residues with BDs can effectively block the transcription of genes that promote cancer cell proliferation [12–14]. Thus, BRD4 has become a possible target for the treatment of various malignancies.

Currently, several inhibitors have been developed for BRD4, and inhibitors have entered clinical trials, for example, JQ1, OTX-015, and I-BET762 [15–18]. Most of the previously reported inhibitors have similar affinity to BD1 and BD2 of BRD4. They have shown good antitumor effects in basic studies and preliminary clinical trials in tumors, but there are still some issues and challenges to overcome. Related studies have shown that pan-BRD4 inhibitors may lead to off-targets and create serious safety concerns due to their masking of the effects of individual BD [19, 20]. Although both BD1 and BD2 recognize acetylated lysine residues, BD1 and BD2 exhibit different functions in biological processes [21]. Among them, BD1 is mainly responsible for chromatin-binding module, while BD2 is utilized to recruit various factors [22, 23]. Studies have shown that inhibitors selectively targeting BD1 or BD2 may provide more effective treatment options. It is reported that selective inhibition of BD1 promotes differentiation of oligodendrocyte progenitors, whereas selective inhibition of BD2 is ineffective, and simultaneous inhibition of both hinders differentiation [24–26]. In addition, residue differences in the structural sequences of BD1 and BD2 offer a structural foundation to the design of selective inhibitors against BD1 and BD2 [27]. Several inhibitors selective for BD1 and BD2 have been reported, with BD2-selective inhibitors showing better toleration in clinical trials [21, 28–30]. Therefore, studying the selective mechanism of inhibitor binding to BD1 and BD2 is essential to design effective drugs for the treatment of cancer.

Molecular dynamics (MD) simulations can well explain ligand-receptor interactions [31–45], and binding free energy calculation is an efficient method to evaluate binding affinity [46–57]. Therefore, these two methods are widely utilized to investigate molecular mechanism of selective binding of inhibitors to receptors [58–63]. Nevertheless, conventional MD (cMD) simulations may trap the conformation in the local minimum space, leading to inadequate conformational samplings. Related literature shows that sufficient conformational samplings can be obtained using multiple replicas MD (MRMD) simulations compared to single lengthy MD simulation [64–72]. Therefore, we use MRMD simulations to investigate the binding selectivity of inhibitors for BD1 and BD2. In this work, we select three inhibitors, SG3-179, GSK778, and GSK620 to achieve the goal. FIG. 1(A–E) shows the structures of the complexes, the binding pockets of BD1 and BD2, and the structures of SG3-179, GSK778, and GSK620. Inhibitors GSK778 and GSK620 have different inhibiting activities against BD1 and BD2. Inhibiting ability of GSK778 and GSK620 on BD1 are scaled in IC_{50} values of 40 and 15800 nmol/L, respectively, while the IC_{50} values of these two inhibitors on BD2 are 6300 and 79 nmol/L, respectively [28, 73]. The IC_{50} value of SG3-179 for BD1 is 21 nmol/L [74], but the IC_{50} value of SG3-179 to BD2 is not available. Thus, to explore the selective mechanism of inhibitors to BD1 and BD2 remains crucial to the design of efficient and selective inhibitors for BD1 and BD2. This study integrates MRMD simulations, dynamics cross-correlation matrix (DCCM) [75], calculations of binding free energies and principal component analysis (PCA) [76–78] to investigate the selective mechanism of inhibitor binding to BD1 and BD2. This research may provide helpful theoretical information for designing inhibitors with high selectivity for BD1 and BD2.

II. METHODS

A. Construction of the system

The initial structures of the SG3-179/BD1,

DOI: 10.1063/1674-0068/cjcp2208126

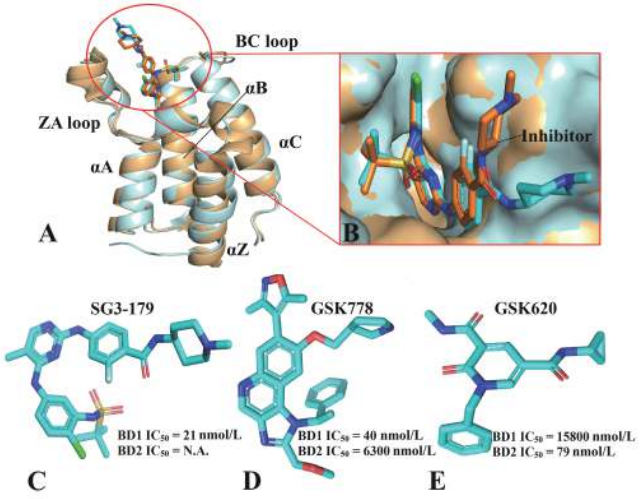

FIG. 1 Molecular structures of inhibitors and proteins: (A) the superimposed structures of BD1 (cyan) with BD2 (orange); (B) the superimposed structures of inhibitor in the binding pocket; (C), (D), and (E) the molecular structures of the inhibitors SG3-179, GSK778, and GSK620 with their potencies (IC_{50}) to BD1 and BD2 of BRD4, respectively.

GSK778/BD1, GSK620/BD1, and SG3-179/BD2 complexes are obtained from the Protein Data Bank (PDB ID: 5F63 [74], 6SWN [28], 6ZB3 [73], and 7KO0 [79]), but the initial structures of the GSK778/BD2 and GSK620/BD2 complexes are not available. Given that the crystal structures of BD1 and BD2 are highly similar, the initial structures of the GSK778/BD2 and GSK620/BD2 complexes are generated by superimposing 6SWN and 6ZB3 with 7KO0, respectively, and then deleting SG3-179 and BD1 using PyMol software (https://www.pymol.org). Considering the different numbers of N-terminal residues in BD1 and BD2, residues 56−166 of BD1 and 349−459 of BD2 are used to construct the initial systems. Non-inhibitor molecules and water molecules outside 5 Å of the inhibitor are removed from the starting systems. All missing hydrogen atoms are added via the Leap module. Reasonable protonation states are assigned to residues using the H++ web server [80]. The structures of SG3-179, GSK620, and GSK778 are optimized using the AM1 method, followed by the assignment of BCC charges to each inhibitor atom by the Antechamber module [81, 82]. The TIP3P water model and the protein force field ff14SB are used to generate parameters for water molecules and proteins, respectively. The general amber force field (GAFF) is used to obtain the force field parameters of SG3-179, GSK620, and GSK778 [83]. All systems are placed in an octahedral TIP3P water box, with a buffer of 12.0 Å in each dimension. In 0.15 mol/L NaCl, the appropriate number of counter ions (Cl^-) are added to maintain the simulated systems electrically neutral.

B. MRMD simulation

The initialization of simulated system may cause unreasonable atom-atom contacts, resulting in instability of MD simulations. To eliminate these negative impacts, two stages of energy minimization are performed on the six systems. First, steepest descent minimization and conjugate gradient minimization (2500 steps each) are performed for the protein and inhibitor in the system, while using a harmonic constraint of 2 kcal·mol^{-1}·Å^{-2} to restrain the non-hydrogen atom. Then, 5000 steps energy minimization is performed for the whole system without any constraints. After that, the temperature of each system is ramped up from 0 K to 300 K within 2 ns, followed by a 2 ns equilibration simulation under the *NPT* ensemble. Five replicas MD simulations are executed for each system to obtain full conformation samplings. First, 100-ns MD simulations without restriction are run to relax all systems at constant temperature and pressure (300 K and 1 bar), from which atomic coordinates are recorded every 5 ps. Subsequently, four conformations randomly selected from the previous simulation are utilized as starting structures to run four new MD simulations (100 ns each). The temperature of systems and the chemical bonds between heavy atoms and hydrogen atoms are constrained using the Langevin thermostat (collision frequency of 2.0 ps^{-1}) and the shake algorithm (time step of 2 fs) [84, 85]. The particle mesh Ewald (PME) method is used to calculate long-range electrostatic interactions (EIs) [86, 87]. In addition, the cut-off distance for calculating EIs and van der Waals interactions (VDWIs) is 10 Å. Five replicas MD simulations in this study are run using the pmemd.cuda module [88−90].

C. Binding free energy calculation

The binding ability between inhibitors and receptors is an important basis for evaluating the efficacy of inhibitors. Molecular mechanics Poisson-Boltzmann surface area (MM-PBSA) and molecular mechanics generalized born surface area (MM-GBSA) are effective methods to assess binding free energy [91−96]. Therefore, the binding free energies of SG3-179, GSK778, and

DOI: 10.1063/1674-0068/cjcp2208126

GSK620 to BD1 and BD2 are calculated using the MM-PBSA and MM-GBSA methods with the following equation:

$$\Delta G_{\text{bind}} = \Delta E_{\text{ele}} + \Delta E_{\text{vdW}} + \Delta G_{\text{pol}} + \Delta G_{\text{nonpol}} - T\Delta S \tag{1}$$

in which the first two terms ΔE_{ele} and ΔE_{vdW} respectively denote EIs and VDWIs of SG3-179, GSK778, and GSK620 with BD1 and BD2. ΔG_{pol} represents the polar solvation free energy, while ΔG_{nonpol} represents the nonpolar solvation free energy. And ΔG_{nonpol} is calculated from the solvent-accessible surface area (SASA):

$$\Delta G_{\text{nonpol}} = \gamma \times \Delta\text{SASA} + \beta \tag{2}$$

where the values of γ and β are set to 0.005 kcal·mol^{-1}·Å^{-2} and 0.00 kcal/mol in MM-PBSA and MM-GBSA calculations [97, 98], respectively. The last term $-T\Delta S$ represents the change in entropy contribution to inhibitor binding and is evaluated using normal model analysis [99, 100].

D. Dynamics cross-correlation matrix

Dynamic cross-correlation matrix (DCCM) provides important information for studying dynamics properties of receptors. The matrix element C_{ij} describing the motion details between residues is estimated with the following equation [75]:

$$C_{ij} = \frac{\langle \Delta r_i \Delta r_j \rangle}{(\langle \Delta r_i{}^2 \rangle \langle \Delta r_j{}^2 \rangle)^{1/2}} \tag{3}$$

where Δr_i denotes the deviation on average position of the ith Cα atom. In addition, positive values of C_{ij} reflect correlated movement between residues, while negative values characterize anti-correlated movement between residues. The degree of motion is indicated by the color-coded pattern.

E. Principal component analysis

Principal component analysis (PCA) is a powerful tool to study the relationship between the internal motion of receptors and their functions. The atomic coordinates retained in the MRMD trajectory are used to build the position covariance matrix C to realize the PCA [77, 78, 101]. The matrix C describing the positional deviation is given as follows:

$$C = \langle (q_i - \langle q_i \rangle)(q_j - \langle q_j \rangle)^T \rangle, \quad (i, j = 1, 2, \cdots 3N) \tag{4}$$

where q_i is the Cartesian coordinate of the Cα atom in the ith residue. The average value of the trajectory in the equilibrium phase is calculated by superimposing the receptors on the reference structure and using a least-squares fit program to eliminate overall translations and rotations [102, 103]. The matrix C can be diagonalized into the diagonal matrix Λ with the eigenvalue λ_i using the orthogonal transformation matrix T:

$$\Lambda = T^T C T \tag{5}$$

where the eigenvectors describing the motion direction of the structural domain are represented by columns, and each eigenvector is associated with an eigenvalue. The magnitude of motion on eigenvector is represented by an eigenvalue, which describes the total fluctuation of the systems along the associated eigenvector.

III. RESULTS AND DISCUSSION

A. Dynamic properties and structural stability of BD1 and BD2

To achieve reasonable conformational sampling of BD1 and BD2, MRMD simulations are executed for six complex systems. Root-mean-square deviations (RMSDs) are an effective method to detect the stability of the simulated system. To assess the convergence of the MRMD simulations, the RMSDs of the backbone atoms in BD1 and BD2 relative to their crystal structure are calculated (FIG. S1 in Supplementary materials, SM). As can be seen in FIG. S1(SM), the RMSDs of all replicas show relatively stable fluctuations in the MRMD simulations, with structural fluctuations kept within the range of 0.5–2.0 Å. After initiating MRMD simulations for 60 ns, all simulated trajectories reach equilibrium and remain stable (FIG. S1 in SM). Hence, the equilibrium portions (60–100 ns) of five replicas are combined to obtain a single connected trajectory (SCT) of 200 ns for subsequent calculations and dynamics analysis.

The structural flexibility of the proteins can be described by root-mean-square fluctuations (RMSFs). We calculate the RMSFs of the Cα atoms in BD1 and BD2 to understand impacts of inhibitor binding on structural flexibility of these two proteins (FIG. 2). The results show that the fluctuating trends of the RMSFs of the two proteins are similar, implying the same flexible regions of BD1 and BD2. The structural domains of the helices are more rigid than the loop regions through the entire MRMD simulations. Significant differences in

DOI: 10.1063/1674-0068/cjcp2208126

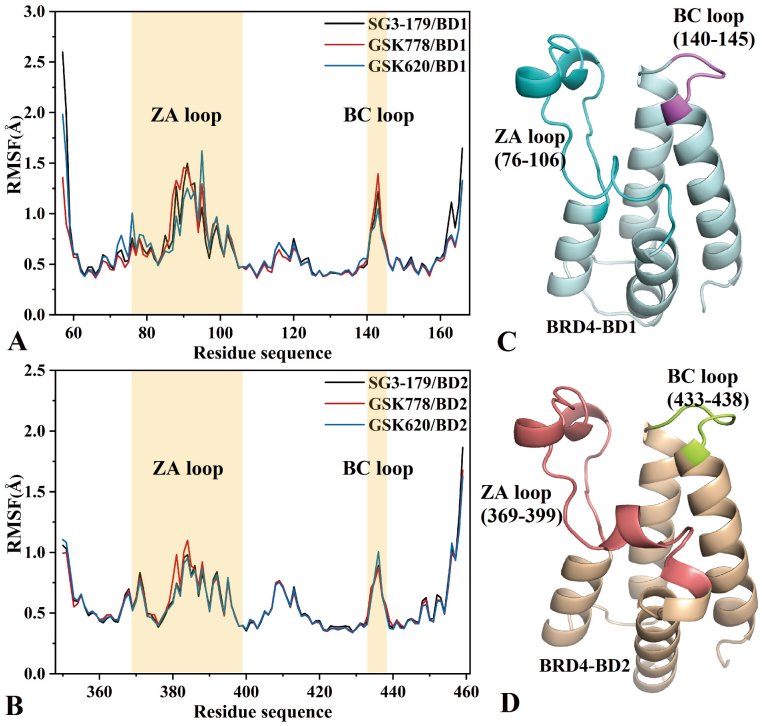

FIG. 2 Root-mean-square fluctuations (RMSFs) of the Cα atoms in BD1 and BD2. (A) SG3-179, GSK778, and GSK620 binding to BD1, (B) SG3-179, GSK778, and GSK620 binding to BD2, (C) and (D) are the ZA and BC loops in BD1 and BD2, respectively.

RMSFs are found in the ZA loop (76–106 for BD1 and 369–399 for BD2) as well as the BC loop (140–145 for BD1 and 433–438 for BD2), except for the N-terminal and C-terminal (FIG. 2 and FIG. S2 in SM). The RMSFs of the ZA and BC loops in BD2 are lower than those in BD1, suggesting that these loops in BD1 are more flexible than those in BD2. Structurally, the ZA and BC loop regions are located near the binding pockets, and some residues within the ZA and BC loops may be key residues for the selective binding of inhibitors to BD1 and BD2 (FIG. 1(A)). To further unveil effects of inhibitor bindings on global flexibility of BD1 and BD2, the molecular surface area (MSA) of six complexes is estimated (FIG. 3). The frequency peaks of the SG3-179/BD1, GSK778/BD1, and GSK620/BD1 complexes are distributed at 6375, 6475, and 6475 Å^2, respectively. While for the SG3-179/BD2, GSK778/BD2, and GSK620/BD2 complexes, the frequency peaks are at 6275, 6325, and 6325 Å^2, respectively, which reveals that the total structural flexibility of BD2 is weaker than that of BD1.

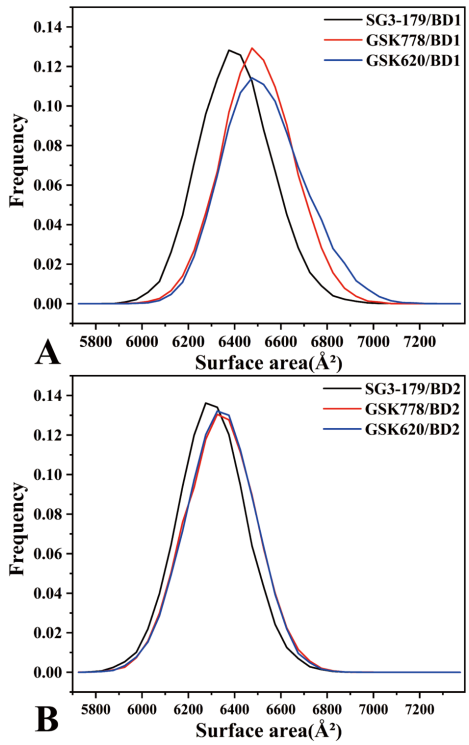

FIG. 3 Frequency distribution of molecular surface areas of BD1 and BD2. (A) BD1 and (B) BD2.

The impact of inhibitor binding on dynamic properties of BD1 and BD2 is explored using DCCM (FIG. 4). The findings suggest that inhibitor bindings alter the movement patterns of BD1 and BD2. Compared with the SG3-179/BD1 (FIG. 4(A)), binding of SG3-179 attenuates the anti-correlated motion occurring in the R1, R3, and R4 regions of BD2, and the correlated motion

DOI: 10.1063/1674-0068/cjcp2208126

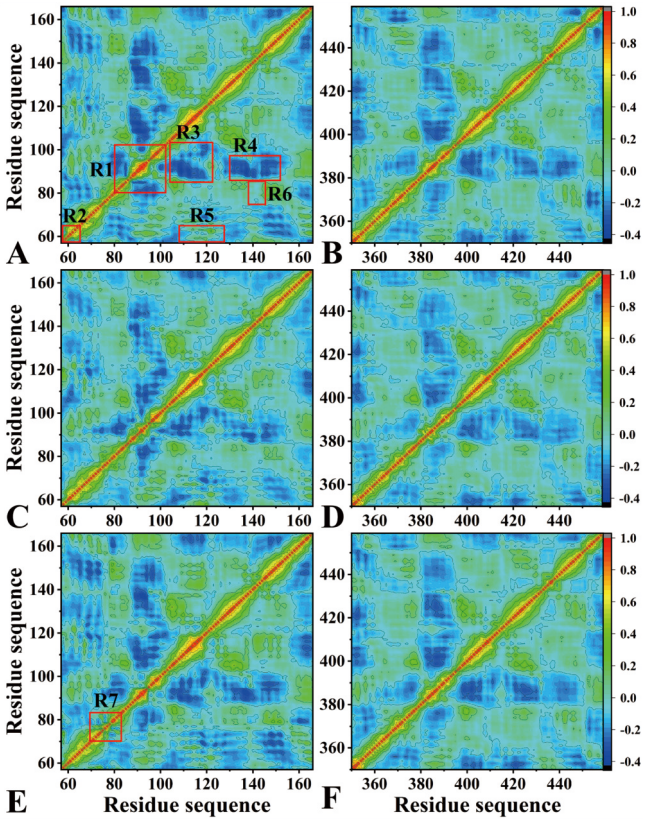

FIG. 4 Dynamic cross-correlation matrix reflects the relative motion between residues in BD1 and BD2. (A), (C), and (E) SG3-179, GSK778, and GSK620 bound to BD1, respectively; (B), (D), and (F) SG3-179, GSK778, and GSK620 bound to BD2, respectively.

in the R5 and R6 regions (FIG. 4(B)). And compared to the GSK778/BD1 (FIG. 4(C)), the presence of GSK778 in the BD2 also slightly weakens the anti-correlated motions of R1, R3, and R4, but softly enhances the correlated movement in the R2 region and the anti-correlated motions in the R5 and R6 regions (FIG. 4(D)). By referencing the GSK620/BD1 (FIG. 4(E)), the binding of GSK620 softly diminishes the anti-correlated motions of R1 and R4, but slightly increases the correlated motion of R7 region (FIG. 4(F)). The aforementioned regions with evident changes in movement patterns are in basic consistence with the regions with obvious changes in structural flexibility from the previous RMSF analysis. Therefore, some residues situated in the regions with significant differences in structural flexibility and dynamics behavior may lead to marked differences in inhibitor interactions with BD1 and BD2.

B. Conformational analysis of BD1 and BD2

PCA is performed on the SCT to uncover conformational changes in BD1 and BD2 caused by inhibitor binding. PCA is achieved by the following steps: (1) constructing the covariance matrix using the Cα atomic coordinates recorded in the SCT, (2) obtaining eigenvalues and eigenvectors by diagonalizing the covariance matrix, (3) visualizing the eigenvectors using VMD software and the molecular structures of BD1 and BD2, and (4) constructing the free energy landscape (FEL) by projecting the SCT onto the first two eigenvectors as reaction coordinates.

As shown in FIG. S3 (SM), the first six eigenvalues of the SG3-179/BD1, GSK778/BD1, and GSK620/BD1 systems account for 64.06%, 55.95%, and 59.83% of the total motion from the SCT, respectively, while the SG3-179/BD2, GSK778/BD2, and GSK620/BD2 systems occupy 55.52%, 51.35%, and 53.95% of the total motion, respectively. The results indicate that the total motion intensity of BD1 is stronger than that of BD2 when bound by the same inhibitor.

FIG. 5 shows the motion direction and motion intensity along the first eigenvectors of BD1 and BD2 obtained by PCA, where FIG. 5(A, C, and E) show concerted motions of BD1 bound by SG3-179, GSK778, and GSK620, respectively, and FIG. 5(B, D, and F) display collective movements of BD2 complexed with SG3-179, GSK778, and GSK620, respectively. The results suggest that inhibitor binding exert different effects on the collective movement of BD1 and BD2, especially in the domains ZA and BC loops (FIG. 5). Compared with the SG3-179/BD1, the binding of SG3-179 to BD2 not only reduces the movement strength of the ZA loop, but also shifts the BC loop outward (FIG. 5 (A) and (B)). Compared to the GSK778/BD1 (FIG. 5(C)), the binding of GSK778 to BD2 largely affects the movement intensity and movement direction of the ZA loop, also changes the movement direction of four α-helices (FIG. 5(D)). By referencing the GSK620/BD1 (FIG. 5(E)), the binding of GSK620 to BD2 obviously alters the concerted motion of BD2. The binding of GSK620 to BD2 not only shifts the ZA loop downward and to the right but also inhibits the movement intensity of this loop relative to the GSK620/BD1. In addition, the movement directions of the BC loop and N-terminal residues of BD2 are changed by the GSK620 binding compared to the GSK620 binding to BD1 (FIG. 5 (E) and (F)). The above analysis shows that the inhibitor binding significantly affects the movement trends of BD1 and BD2, and these results are consis-

DOI: 10.1063/1674-0068/cjcp2208126

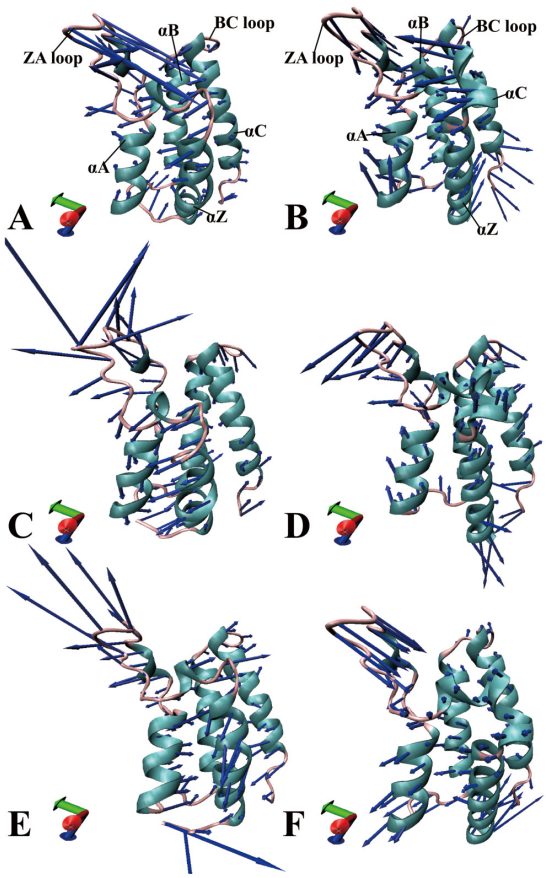

FIG. 5 Collective motions of BD1 and BD2 correspond to the first eigenvector PC1. (A), (C), and (E) respectively correspond to SG3-179, GSK778, and GSK620 complexed with BD1; (B), (D), and (F) respectively correspond to SG3-179, GSK778, and GSK620 complexed with BD2.

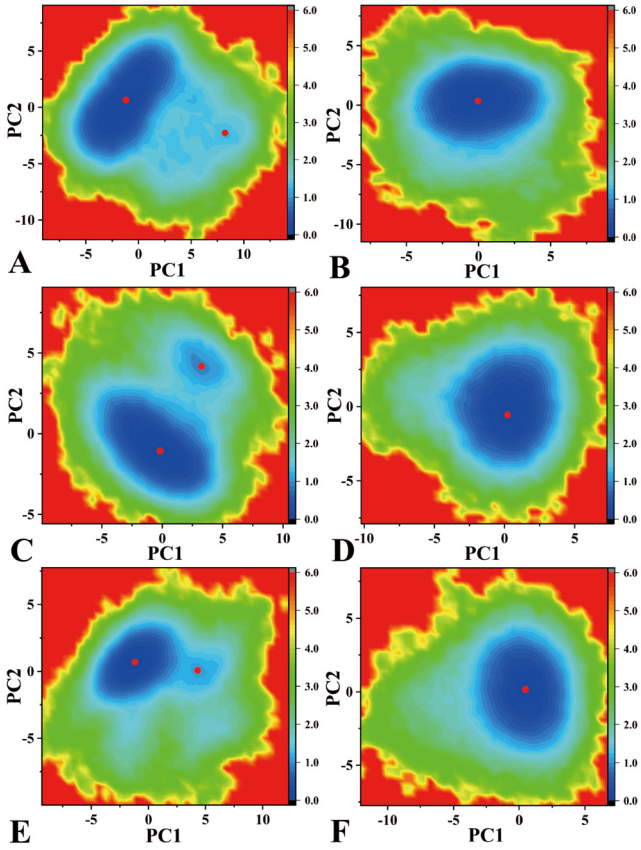

FIG. 6 Free energy landscapes of BD1 and BD2 constructed by projecting the MRMD trajectories onto PC1 and PC2. (A) SG3-179 bound to BD1, (B) SG3-179 bound to BD2, (C) GSK778 bound to BD1, (D) GSK778 bound to BD2, (E) GSK620 bound to BD1, and (F) GSK620 bound to BD2.

tent with the studies of Wang *et al.* [68] and Su *et al.* [92].

The free energy landscapes of BD1 and BD2 are shown in FIG. 6. The results reveal that inhibitor binding induces different free energy profiles for BD1 and BD2. For the binding of SG3-179, GSK778, and GSK620 to BD1, BD1 mainly generates two free energy basins (FIG. 6(A, C, and E)). However, for the binding of SG3-179, GSK778, and GSK620 to BD2, the conformation of BD2 is mainly concentrated in one subspace (FIG. 6(B, D and F)). The above analysis indicates that inhibitor binding leads to conformational rearrangements of BD1 and BD2, and that the conformation of BD2 is more stable than that of BD1.

C. Binding ability of inhibitors to BD1 and BD2

To understand energetic basis of the selective binding of inhibitors toward BD1 and BD2, the binding free energies of six complexes are computed by the MM-PBSA and MM-GBSA methods based on 500 snapshots selected in the SCT. In addition, 100 snapshots are selected from the 500 snapshots to estimate the entropy contribution. Table I and Table S1 in SM show the results of the MM-PBSA and MM-GBSA computations, respectively. It can be seen that the predicted values of binding free energies of SG3-179/BD1, GSK778/BD1, GSK620/BD1, GSK778/BD2, and GSK620/BD2 complexes are in good agreement with the experimental values in terms of ranking, which indicates that our free energy analysis is reasonable.

According to Table I and Table S1 in SM, the calculated results of MM-PBSA and MM-GBSA are similar. The polar solvation energy ($\Delta G_{\rm pol}$) shields the electrostatic interaction ($\Delta E_{\rm ele}$), resulting in an unfavorable force ($\Delta G_{\rm ele+pol}$) on the binding of inhibitors to BD1 and BD2. Non-polar solvation free energy ($\Delta G_{\rm nonpol}$) and van der Waals interactions ($\Delta E_{\rm vdW}$) provide favorable forces ($\Delta G_{\rm vdW+nonpol}$) for inhibitors binding. In

DOI: 10.1063/1674-0068/cjcp2208126

TABLE I Binding free energies of inhibitors to BD1 and BD2 calculated by MM-PBSA method. All values are in kcal/mol.

Complexes	ΔE_{ele}	ΔE_{vdW}	ΔG_{pol}	ΔG_{nonpol}	$\Delta G_{ele+pol}$[a]	$\Delta G_{vdW+nonpol}$[b]
SG3-179/BD1	−25.19±0.35	−41.63±0.17	37.90±0.32	−4.21±0.01	12.71±0.15	−45.84±0.12
SG3-179/BD2	−20.16±0.23	−43.50±0.15	33.42±0.22	−4.60±0.01	13.26±0.14	−48.10±0.11
GSK778/BD1	−9.22±0.26	−45.53±0.14	26.77±0.25	−4.48±0.01	17.55±0.14	−50.01±0.10
GSK778/BD2	−8.82±0.19	−44.04±0.15	26.96±0.20	−4.53±0.01	18.14±0.12	−48.57±0.11
GSK620/BD1	−18.53±0.18	−31.35±0.12	30.44±0.14	−3.66±0.01	11.91±0.15	−35.01±0.09
GSK620/BD2	−23.84±0.19	−36.07±0.12	34.10±0.14	−3.95±0.01	10.26±0.15	−40.02±0.09
Complexes	ΔH	$-T\Delta S$	ΔG_{bind}	IC_{50}/(nmol/L)	ΔG_{exp}[c]	
SG3-179/BD1	−33.13±0.19	21.75±0.64	−11.38	21	−10.57	
SG3-179/BD2	−34.84±0.15	24.14±0.73	−10.70	–[d]		
GSK778/BD1	−32.46±0.17	21.85±0.85	−10.61	40	−10.19	
GSK778/BD2	−30.43±0.14	22.73±0.67	−7.70	6300	−7.16	
GSK620/BD1	−23.10±0.13	16.75±0.67	−6.35	15800	−6.61	
GSK620/BD2	−29.76±0.15	19.85±0.66	−9.91	79	−9.78	

[a] $\Delta G_{ele+pol} = \Delta E_{ele} + \Delta G_{pol}$.
[b] $\Delta G_{vdW+nonpol} = \Delta E_{vdW} + \Delta G_{nonpol}$.
[c] The experimental values are calculated from the equation: $\Delta G_{exp} = -RT\ln(IC_{50})$.
[d] The IC_{50} value is not available.

addition, the change in entropy ($-T\Delta S$) exerts an unfavorable force on the associations of inhibitors with BD1 and BD2. According to Table I, the favorable factor $\Delta G_{vdW+nonpol}$ of the SG3-179/BD2 complex is increased by 2.26 kcal/mol compared to the SG3-179/BD1 complex, while the unfavorable factor $\Delta G_{ele+pol}$ also increases by 0.55 kcal/mol relative to the SG3-179/BD1 complex, resulting in the binding enthalpy (ΔH) of the SG3-179/BD2 complex enhanced by 1.71 kcal/mol compared with the SG3-179/BD1 one. However, compared to the SG3-179/BD1 complex, the value of $-T\Delta S$ for the SG3-179/BD2 one is enhanced by 2.39 kcal/mol. Thus, the total energy (ΔG_{bind}) of SG3-179/BD2 complex is reduced by 0.68 kcal/mol by referencing that of SG3-179 to BD1, indicating that SG3-179 prefers to bind to BD1. For the inhibitor GSK778, compared to the GSK778/BD1 complex, the favorable contribution $\Delta G_{vdW+nonpol}$ is decreased by 1.44 kcal/mol and the unfavorable contribution $\Delta G_{ele+pol}$ is enhanced by 0.59 kcal/mol for the GSK778/BD2 complex, causing the ΔH of the GSK778/BD2 one decreased by 2.03 kcal/mol. Meanwhile, the $-T\Delta S$ value of the GSK778/BD2 complex is increased by 0.88 kcal/mol compared to the GSK778/BD1 complex, resulting in the ΔG_{bind} of GSK778/BD2 decreased by 2.91 kcal/mol, which demonstrates that GSK778 prefers to bind to BD1. In the case of the inhibitor GSK620, the $\Delta G_{vdW+nonpol}$ of the GSK620/BD2 complex is increased by 5.01 kcal/mol compared with the GSK620/BD1 one, while the unfavorable $\Delta G_{ele+pol}$ is decreased by 1.65 kcal/mol, causing the ΔH of the GSK620/BD2 complex increased by 6.66 kcal/mol relative to the GSK620/BD1 one. Although the $-T\Delta S$ of the GSK620/BD2 complex is increased by 3.10 kcal/mol compared to the GSK620/BD1 one, the ΔG_{bind} of the GSK620/BD2 complex is increased by 3.56 kcal/mol compared to GSK620/BD1 one, indicating that GSK620 prefers to bind to BD2. The above analyses suggest that van der Waals interactions provide the major energetic contribution to inhibitor binding. Furthermore, electrostatic interactions and entropy changes are also key factors for the selective binding of inhibitors to BD1 and BD2.

D. Interaction mechanism of inhibitor binding to BD1 and BD2

To comprehend molecular mechanism of inhibitor selection for BD1 and BD2, the total binding free energies of six complexes are decomposed into the energy contributions of individual residues using the residue-based free energy decomposition method (FIG. S4 in

DOI: 10.1063/1674-0068/cjcp2208126

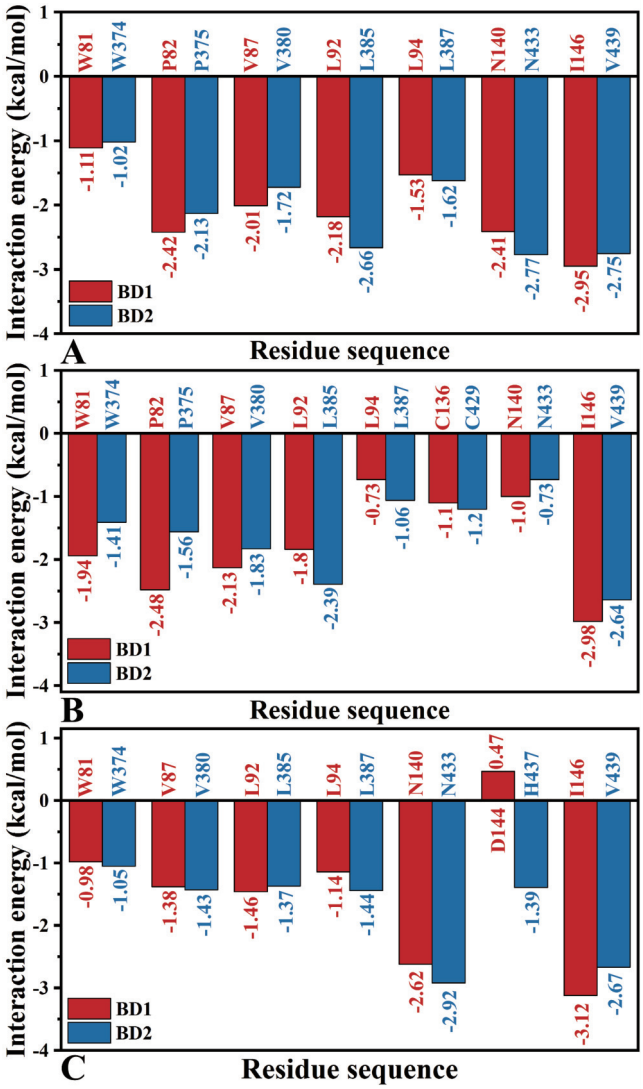

FIG. 7 Energy contribution of key residues in BD1 and BD2. (A) SG3-179, (B) GSK778, and (C) GSK620.

SM). Meanwhile, the differences between residues at corresponding positions on BD1 and BD2 are calculated (FIG. S5 in SM). FIG. 7 depicts the residues of significant contributions to inhibitor binding. The energy contribution of hot spot residues is decomposed to further analyze the binding mechanism of inhibitors to BD1 and BD2. In addition, the hydrogen bonding interactions (HBIs) between the inhibitors with BD1 and BD2 are analyzed (Table II). FIGs. 8–10 show the hydrophobic contacts and HBIs between SG3-179, GSK778, and GSK620 with hot spot residues.

For SG3-179 binding to BD1 and BD2, FIG. 7(A) and FIG. S5(A) in SM show the seven residues W81, P82, V87, L92, L94, N140, and I146 that produce interaction energies greater than 1.0 kcal/mol for SG3-179 bound to BD1. The energy contributions of these seven residues are −1.11, −2.42, −2.01, −2.18, −1.53, −2.41, and −2.95 kcal/mol, respectively. According to FIG. 8(A), the interaction energies of SG3-179 with V87, L92, L94, and I146 are mainly from van der Waals interactions, which are structurally consistent with the CH–π interactions between the hydrophobic ring of SG3-179 with the alkyls of V87, L92, L94, and I146 (FIG. 8(B)). In addition, the favorable contributions of SG3-179 with W81 and P82 are also mainly from van der Waals interactions (FIG. 8(A)). Structurally, SG3-179 with W81 and P82 produces the π–π interactions, and a stable hydrogen bond (HB) is formed between P82 and SG3-179 (SG3-179-N16-H15···P82-O) with an occupancy of 65.25% (FIG. 8(B) and Table II). The interaction energy of SG3-179 and N140 mainly arises from electrostatic interactions, which is associated with the formation of two stable HBs between SG3-179 and N140, including N140-ND2-HD21···SG3-179-N21 and SG3-179-N23-H19···N140-OD1 with occupancies of 99.49% and 88.96%, respectively (Table II and FIG. 8(B)). According to FIG. S5(B) in SM, FIG. 6(C, D) and Table II, the binding pattern of SG3-179/BD2 is similar to that of SG3-179 to BD1. In addition, eight pairs of residues (P82, P375), (Q85, K378), (V87, V380), (L92, L385), (N93, G386), (N140, N433), (D144, H437), and (M149, M442) in (BD1, BD2) produce energy differences greater than 0.25 kcal/mol for the binding of SG3-179 (FIG. S5(A)), suggesting that these residues play crucial roles in the selective binding of SG3-179 to BD1 and BD2.

For the binding of GSK778 with BD1 and BD2, according to FIG. 7(B) and FIG. S5(C) in SM, the favorable interaction energies of GSK778 with seven residues in BD1 are stronger than 1.0 kcal/mol. These seven residues are W81, P82, V87, L92, C136, N140, and I146, which provide the energetic contributions of −1.94, −2.84, −2.13, −1.8, −1.10, −1.00, and −2.98 kcal/mol for the binding of GSK778 to BD1, respectively. As shown in FIG. 9(A), the interaction energy of GSK778 with W81, P82, V87, L92, C136, and I146 is mainly from van der Waals interactions. It can be seen that the hydrophobic rings of W81 and P82 as well as the alkyl groups of V87, L92, C136, and I146 in BD1 are structurally close to the hydrophobic ring of GSK778, hence they easily generate the π–π interactions and the CH–π interactions (FIG. 9(B)). In addition, W81 and GSK778 produce an HB (W81-NE1-HE1···GSK778-O05) with an occupancy of 36.96% (Table II). The strong electrostat-

DOI: 10.1063/1674-0068/cjcp2208126

TABLE II Hydrogen bonds between inhibitors with BD1 and BD2.

Complexes	Hydrogen bonds[a]	Distance/Å	Angle/(°)	Occupancy/%
SG3-179/BD1	N140-ND2-HD21···SG3-179-N21	2.96	162.9	99.49
	SG3-179-N23-H19···N140-OD1	3.09	160.8	88.96
	SG3-179-N16-H15···P82-O	3.13	145.3	65.25
SG3-179/BD2	N433- ND2-HD21···SG3-179-N21	2.98	162.1	99.87
	SG3-179-N23-H19···N433-OD1	2.98	162.2	99.13
	SG3-179-N16-H15···P375-O	3.26	147.0	30.34
GSK778/BD1	N140-ND2-HD21···GSK778-O26	3.17	154.2	81.38
	N140-ND2-HD22···GSK778-N25	3.18	142.14	74.68
	W81-NE1-HE1···GSK778-O05	2.99	148.7	36.96
GSK778/BD2	N433- ND2-HD21···GSK778-O26	3.18	149.9	73.64
	N433- ND2-HD21···GSK778-N25	3.23	140.6	57.46
GSK620/BD1	N140-ND2-HD21···GSK620-O08	2.93	163.3	99.23
	GSK620-N34-H14···N140-OD1	3.01	146.8	91.48
GSK620/BD2	N433- ND2-HD21···GSK620-O08	2.96	164.3	99.30
	GSK620-N34-H14···N433-OD1	2.93	153.4	99.25

[a] Hydrogen bonding is defined as an acceptor···H-donor angle of >120° and an acceptor···donor distance <3.5 Å.

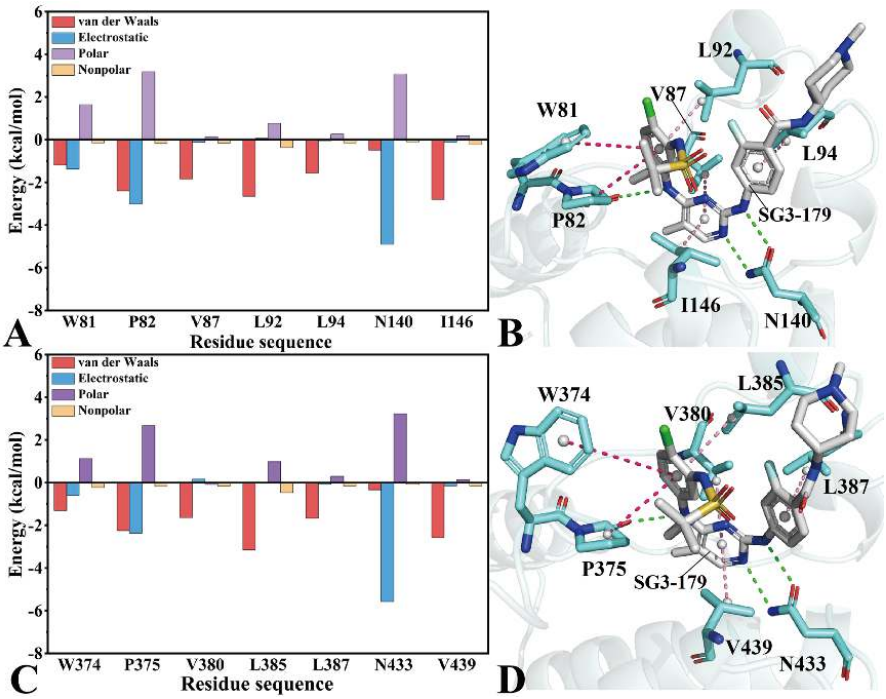

FIG. 8 Energy decomposition of hot spot residues and interactions network in the SG3-179 bound to BD1/BD2. (A, B) SG3-179 bound to BD1, and (C, D) SG3-179 bound to BD2. Hydrogen bonds (green), CH–π (pink) and π–π (hot pink).

ic interactions between GSK778 and N140 in BD1 are consistent with the formation of two stable HBs between GSK778 and N140 (N140-ND2-HD21···GSK778-O26 and N140-ND2-HD22···GSK778-N25) with occupancies of 81.38% and 74.68%, respectively (Table II and FIG. 9(B)). The interaction mechanism of GSK778 binding to BD2 is similar to that of GSK778 bound to BD1 (FIG. S4(D), FIG. 9(C, D), and Table II). However, corresponding to residue W81 in BD1, the HBI between residue W374 and GSK778 in BD2 disappears, and the energy contribution of W374 is decreased by 0.53 kcal/mol relative to W81, which suggests that the HBI of the inhibitor with BD1 and BD2 is critical for the selective binding of the inhibitor. Furthermore,

DOI: 10.1063/1674-0068/cjcp2208126

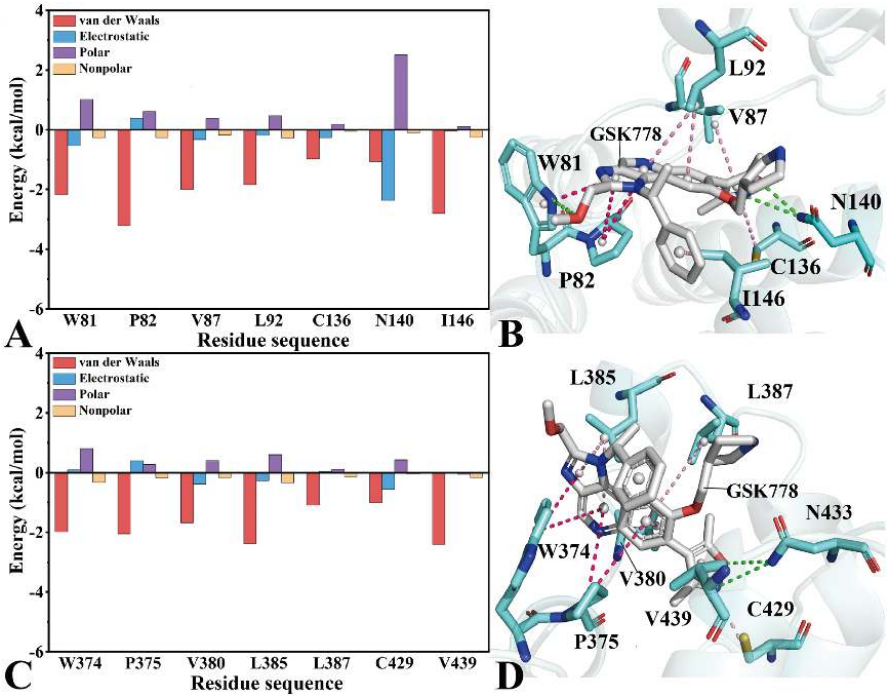

FIG. 9 Energy decomposition of hot spot residues and interactions network in the GSK778 bound to BD1 or BD2. (A, B) GSK778 bound to BD1, and (C, D) GSK778 bound to BD2. Hydrogen bonds (green), CH–π (pink) and π–π (hot pink).

FIG. S5(B) shows that the interaction energies of GSK778 with P375, Q378, V380, N433, and V439 in BD2 are decreased by 0.92, 0.68, 0.30, 0.27, and 0.34 kcal/mol, respectively, compared to the comparable residues in BD1. Therefore, these residues and the corresponding residues in BD1 are essential for the selective binding of GSK778 to BD1 over BD2.

Regarding the binding of GSK620 to BD1 and BD2, according to FIG. 7(C) and FIG. S5(E) in SM, the interaction energies of GSK620 with five residues V87, L92, L94, N140, and I146 are greater than 1.0 kcal/mol. The energy contributions of these five residues to the binding of GSK620 to BD1 are −1.38, −1.46, −1.14, −2.62, and −3.12 kcal/mol, respectively. As seen in FIG. 10(A), the favorable energies of GSK620 with V87, L92, L94, and I146 are primarily from van der Waals interactions. Structurally, the hydrophobic rings of GSK620 with the alkyl groups of V87, L92, L94, and I146 produce CH–π interactions (FIG. 10(B)). The favorable energies of GSK620 with N140 are primarily from electrostatic interactions, which structurally agrees with the formation of two stable HBs between GSK620 and N140, including N140-ND2-HD21···GSK620-O08 and GSK620-N34-H14···N140-OD1 with the occupancies of 99.23% and 91.48%, respectively (Table II and FIG. 10(D)). Compared to the GSK620 bound to BD1, seven residues P375, V380, L385, L387, N433, H437, and V439 in BD2 provide stronger interaction energies by 1.0 kcal/mol for the binding of GSK620 to BD2 (FIG. 7(C) and FIG. S5(F) in SM). Structurally, residues P375, V380, L385, L387, H437, and V439 with GSK620 form multiple hydrophobic interactions, and residue N433 with GSK620 produces two HBIs (FIG. 10(D)). The differences in the interactions of GSK620 with residues (P82, P375), (V87, V380), and (L92, L385) in (BD1, BD2) are less than 0.10 kcal/mol (FIG. 7(C)), indicating that these residues hardly provide contributions for the binding selectivity of GSK620 to BD1 and BD2. As seen in FIG. S5(C) in SM, relative to the energies provided by residues W81, L94, N140, K141, and D144 in BD1 for GSK620 binding to BD1, the interaction energies provided by residues W374, L387, N433, P434, and H437 in BD2 for GSK620 binding to BD2 are enhanced by 0.35, 0.30, 0.30, 0.48, and 1.86 kcal/mol, respectively. Thus, these residues are responsible for the selective binding of GSK620 to BD2 over BD1.

According to the above analysis, the hot spot residues (W81, W374), (P82, P375), (V87, V380), (L92, L385), (L94, L387), (C136, C429), (N140, N433), (D144, H437), and (I146, V439) of (BD1, BD2) provide the major energy contributions to inhibitors binding to BD1 and BD2. In addition, residues (Q85, K378), (N93, G386), and (K141, P434) of (BD1, BD2) provide signifi-

DOI: 10.1063/1674-0068/cjcp2208126

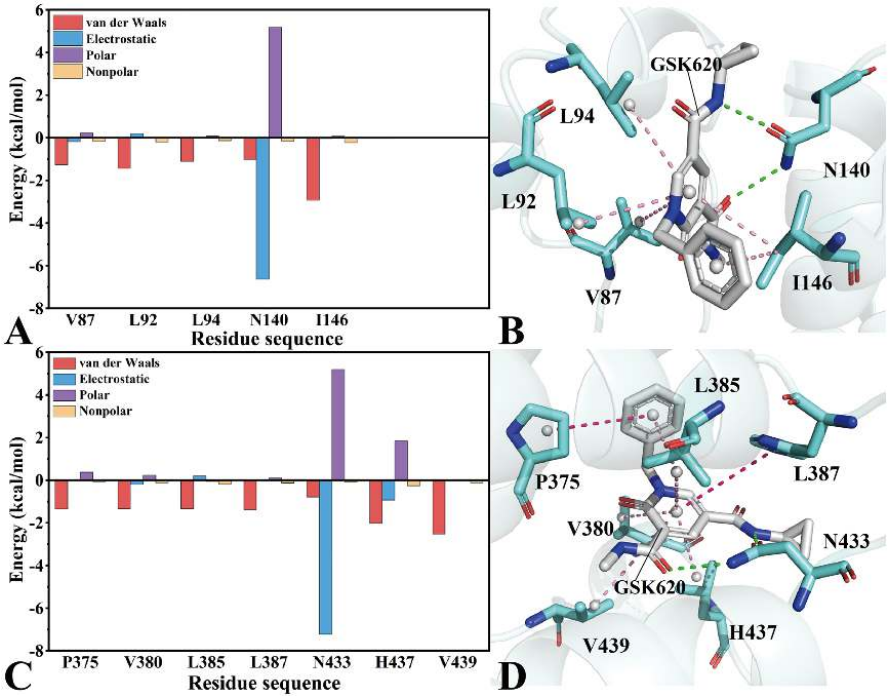

FIG. 10 Energy decomposition of hot spot residues and interactions network in the GSK620 bound to BD1 or BD2. (A, B) GSK620 bound to BD1, and (C, D) GSK620 bound to BD2. Hydrogen bonds (green), CH–π (pink) and π–π (hot pink).

cant energy differences in the binding of inhibitors. Therefore, these residues may be effective targets for the development of selective BD1 or BD2 inhibitors. Meanwhile, hydrophobic interactions and HBIs are two main forces with BD1 and BD2, thus the rational optimization of these two interactions may hopefully improve the selectivity of the inhibitor for BD1 and BD2.

IV. CONCLUSION

In the present work, we perform 500 ns MRMD simulations (five replicas) on six systems of BD1 and BD2 bound by SG3-179, GSK778, and GSK620 to decipher the selective mechanism of inhibitors toward BD1 and BD2. The RMSFs and DCCMs of the Cα atoms from BD1 and BD2 are calculated based on the single connected trajectory, and the results show that BD1 has greater structural flexibility than BD2, meanwhile both of them exhibit distinct internal dynamics behaviors. In addition, the results of PCA uncover that binding of the inhibitors lead to different changes in the motions of the ZA and BC loops of BD1 and BD2. Binding free energies of SG3-179, GSK778, and GSK620 to BD1 and BD2 calculated by MM-PBSA and MM-GBSA methods suggest that SG3-179 and GSK778 can more favorably bind to BD1 than BD2, while GSK620 is more selective for BD2 over BD1. Calculations of the energy differences of the corresponding residues show that residues (W81, W374), (P82, P375), (Q85, K378), (V87, V380), (L92, L385), (N93, G386), (L94, L387), (C136, C429), (N140, N433), (K141, P434), (D144, H437) and (I146, V439) corresponding to (BD1, BD2) provide significant energy differences for SG3-179, GSK778 and GSK620 binding to BD1 and BD2, which can be used as effective targets for designing high selective inhibitor against BD1 and BD2. In addition, the CH–π, π–π, and hydrogen bonding interactions provide important energetic contributions to the binding of inhibitors to BD1 and BD2. This study provides insight into the selective mechanism of inhibitors with BD1 and BD2 and offers theoretical guidance for the design of highly selective inhibitors toward BD1 and BD2.

Supplementary materials: Binding free energies of inhibitors to BD1 and BD2 calculated by the MM-GBSA (Table S1); RMSDs of six complexes of BD1 and BD2 bound by SG3-179, GSK778, and GSK620 (FIG. S1); ΔRMSF of BD1 and BD2 (FIG. S2); eigenvalues of the complexes (FIG. S3); energy contribution of per-residues (FIG. S4); energy difference of the corresponding residues of BD1 and BD2 (FIG. S5) are given.

V. ACKNOWLEDGEMENTS

This work is supported by the National Natural Sci-

ence Foundation of China (No.11274205, No.11274206, and No.11504206), Natural Science Foundation of Shandong Province (ZR2022MA016, ZR2020ME231), and Key Research and Development Project of Shandong province (No.2019GGX102050).

[1] A. C. Belkina and G. V. Denis, Nat. Rev. Cancer **12**, 465 (2012).
[2] P. Filippakopoulos and S. Knapp, FEBS Lett. **586**, 2692 (2012).
[3] Z. Yang, J. H. N. Yik, R. Chen, N. He, M. K. Jang, K. Ozato, and Q. Zhou, Mol. Cell **19**, 535 (2005).
[4] T. Fujisawa and P. Filippakopoulos, Nat. Rev. Mol. Cell Bio. **18**, 246 (2017).
[5] E. Ferri, C. Petosa, and C. E. McKenna, Biochem. Pharmacol. **106**, 1 (2016).
[6] P. Filippakopoulos, S. Picaud, M. Mangos, T. Keates, J. P. Lambert, D. Barsyte Lovejoy, I. Felletar, R. Volkmer, S. Müller, T. Pawson, A. C. Gingras, C. H. Arrowsmith, and S. Knapp, Cell **149**, 214 (2012).
[7] S. Y. Wu and C. M. Chiang, J. Biol. Chem. **282**, 13141 (2007).
[8] X. Tang, R. Peng, J. E. Phillips, J. Deguzman, Y. Ren, S. Apparsundaram, Q. Luo, C. M. Bauer, M. E. Fuentes, J. A. DeMartino, G. Tyagi, R. Garrido, C. M. Hogaboam, C. P. Denton, A. M. Holmes, C. Kitson, C. S. Stevenson, and D. C. Budd, Am. J. Pathol. **183**, 470 (2013).
[9] O. Goundiam, P. Gestraud, T. Popova, T. De la Motte Rouge, V. Fourchotte, D. Gentien, P. Hupé, V. Becette, C. Houdayer, S. Roman-Roman, M. H. Stern, and X. Sastre-Garau, Int. J. Cancer **137**, 1890 (2015).
[10] X. Mu, L. Bai, Y. Xu, J. Wang, and H. Lu, Biochem. Bioph. Res. Co. **521**, 833 (2020).
[11] C. A. French, C. L. Ramirez, J. Kolmakova, T. T. Hickman, M. J. Cameron, M. E. Thyne, J. L. Kutok, J. A. Toretsky, A. K. Tadavarthy, U. R. Kees, J. A. Fletcher, and J. C. Aster, Oncogene **27**, 2237 (2008).
[12] S. Mujtaba, L. Zeng, and M. M. Zhou, Oncogene **26**, 5521 (2007).
[13] S. G. Smith and M. M. Zhou, ACS Chem. Biol. **11**, 598 (2016).
[14] Y. Duan, Y. Guan, W. Qin, X. Zhai, B. Yu, and H. Liu, MedChemComm **9**, 1779 (2018).
[15] P. Filippakopoulos, J. Qi, S. Picaud, Y. Shen, W. B. Smith, O. Fedorov, E. M. Morse, T. Keates, T. T. Hickman, I. Felletar, M. Philpott, S. Munro, M. R. McKeown, Y. Wang, A. L. Christie, N. West, M. J. Cameron, B. Schwartz, T. D. Heightman, N. La Thangue, C. A. French, O. Wiest, A. L. Kung, S. Knapp, and J. E. Bradner, Nature **468**, 1067 (2010).
[16] C. Berthon, E. Raffoux, X. Thomas, N. Vey, C. Gomez Roca, K. Yee, D. C. Taussig, K. Rezai, C. Roumier, P. Herait, C. Kahatt, B. Quesnel, M. Michallet, C. Recher, F. Lokiec, C. Preudhomme, and H. Dombret, Lancet Haematol. **3**, e186 (2016).
[17] O. Mirguet, R. Gosmini, J. Toum, C. A. Clément, M. Barnathan, J. M. Brusq, J. E. Mordaunt, R. M. Grimes, M. Crowe, O. Pineau, M. Ajakane, A. Daugan, P. Jeffrey, L. Cutler, A. C. Haynes, N. N. Smithers, C. w. Chung, P. Bamborough, I. J. Uings, A. Lewis, J. Witherington, N. Parr, R. K. Prinjha, and E. Nicodème, J. Med. Chem. **56**, 7501 (2013).
[18] T. Lu, W. Lu, and C. Luo, Expert Opin. Ther. Pat. **30**, 57 (2020).
[19] G. Andrieu, A. C. Belkina, and G. V. Denis, Drug Discov. Today Technol. **19**, 45 (2016).
[20] D. B. Doroshow, J. P. Eder, and P. M. LoRusso, Ann. Oncol. **28**, 1776 (2017).
[21] S. Picaud, C. Wells, I. Felletar, D. Brotherton, S. Martin, P. Savitsky, B. Diez Dacal, M. Philpott, C. Bountra, H. Lingard, O. Fedorov, S. Müller, E. Brennan Paul, S. Knapp, and P. Filippakopoulos, Proc. Natl. Acad. Sci. USA **110**, 19754 (2013).
[22] J. Liu, Z. Duan, W. Guo, L. Zeng, Y. Wu, Y. Chen, F. Tai, Y. Wang, Y. Lin, Q. Zhang, Y. He, J. Deng, R. L. Stewart, C. Wang, P. C. Lin, S. Ghaffari, B. M. Evers, S. Liu, M. M. Zhou, B. P. Zhou, and J. Shi, Nat. Commun. **9**, 5200 (2018).
[23] L. T. Wang, S. N. Wang, S. S. Chiou, K. Y. Liu, C. Y. Chai, C. M. Chiang, S. K. Huang, K. K. Yokoyama, and S. H. Hsu, Oncogene **38**, 518 (2019).
[24] C. M. Chiang, Chem. Biol. **21**, 804 (2014).
[25] M. Gacias, G. Gerona Navarro, Alexander N. Plotnikov, G. Zhang, L. Zeng, J. Kaur, G. Moy, E. Rusinova, Y. Rodriguez, B. Matikainen, A. Vincek, J. Joshua, P. Casaccia, and M. M. Zhou, Chem. Biol. **21**, 841 (2014).
[26] C. Galdeano and A. Ciulli, Future Med. Chem. **8**, 1655 (2016).
[27] Y. Liu, X. Wang, J. Zhang, H. Huang, B. Ding, J. Wu, and Y. Shi, Biochemistry **47**, 6403 (2008).
[28] O. Gilan, I. Rioja, K. Knezevic, J. Bell Matthew, M. Yeung Miriam, R. Harker Nicola, Y. N. Lam Enid, C. Chung, P. Bamborough, M. Petretich, M. Urh, J. Atkinson Stephen, K. Bassil Anna, J. Roberts Emma, D. Vassiliadis, L. Burr Marian, G. S. Preston Alex, C. Wellaway, T. Werner, R. Gray James, A. M. Michon, T. Gobbetti, V. Kumar, E. Soden Peter, A. Haynes, J. Vappiani, F. Tough David, S. Taylor, S. J. Dawson, M. Bantscheff, M. Lindon, G. Drewes, H. Demont Emmanuel, L. Daniels Danette, P. Grandi, K. Prinjha Rab, and A. Dawson Mark, Science **368**, 387 (2020).
[29] E. J. Faivre, K. F. McDaniel, D. H. Albert, S. R.

DOI: 10.1063/1674-0068/cjcp2208126

Mantena, J. P. Plotnik, D. Wilcox, L. Zhang, M. H. Bui, G. S. Sheppard, L. Wang, V. Sehgal, X. Lin, X. Huang, X. Lu, T. Uziel, P. Hessler, L. T. Lam, R. J. Bellin, G. Mehta, S. Fidanze, J. K. Pratt, D. Liu, L. A. Hasvold, C. Sun, S. C. Panchal, J. J. Nicolette, S. L. Fossey, C. H. Park, K. Longenecker, L. Bigelow, M. Torrent, S. H. Rosenberg, W. M. Kati, and Y. Shen, Nature **578**, 306 (2020).

[30] G. S. Sheppard, L. Wang, S. D. Fidanze, L. A. Hasvold, D. Liu, J. K. Pratt, C. H. Park, K. Longenecker, W. Qiu, M. Torrent, P. J. Kovar, M. Bui, E. Faivre, X. Huang, X. Lin, D. Wilcox, L. Zhang, Y. Shen, D. H. Albert, T. J. Magoc, G. Rajaraman, W. M. Kati, and K. F. McDaniel, J. Med. Chem. **63**, 5585 (2020).

[31] M. Yang, X. Zhang, and K. Han, Proteins **78**, 2222 (2010).

[32] S. Lu, W. Huang, Q. Wang, Q. Shen, S. Li, R. Nussinov, and J. Zhang, Biophys. J. **108**, 528a (2015).

[33] M. J. Yang, X. Q. Pang, X. Zhang, and K. L. Han, J. Struct. Biol. **173**, 57 (2011).

[34] G. Li, H. Shen, D. Zhang, Y. Li, and H. Wang, J. Chem. Theory Comput. **12**, 676 (2016).

[35] G. Hu, A. Ma, X. Dou, L. Zhao, and J. Wang, Int. J. Mol. Sci. **17**, 819 (2016).

[36] J. Su, X. Liu, S. Zhang, F. Yan, Q. Zhang, and J. Chen, J. Biomol. Struct. Dyn. **36**, 1212 (2018).

[37] J. Chen, X. Wang, L. Pang, J. Z. H. Zhang, and T. Zhu, Nucleic Acids Res. **47**, 6618 (2019).

[38] Q. Wang, Y. Li, J. Xu, Y. Wang, D. Shi, L. Liu, E. L. H. Leung, and X. Yao, Proteins **87**, 3 (2019).

[39] R. Tumdam, A. Kumar, N. Subbarao, and B. S. Balaji, SAR QSAR Environ. Res. **29**, 975 (2018).

[40] S. Chen, Y. He, Y. Geng, Z. Wang, L. Han, and W. Han, Molecules **27**, 118 (2022).

[41] T. Fu, G. Zheng, G. Tu, F. Yang, Y. Chen, X. Yao, X. Li, W. Xue, and F. Zhu, ACS Chem. Neurosci. **9**, 1492 (2018).

[42] J. Wang and Y. Miao, J. Phys. Chem. B **123**, 6462 (2019).

[43] J. Wang, P. R. Arantes, A. Bhattarai, R. V. Hsu, S. Pawnikar, Y. M. Huang, G. Palermo, and Y. Miao, Wires Comput. Mol. Scimol. Sci **11**, e1521 (2021).

[44] Z. Sun, Z. Gong, F. Xia, and X. He, Chem. Phys. **548**, 111245 (2021).

[45] W. Xue, P. Wang, G. Tu, F. Yang, G. Zheng, X. Li, X. Li, Y. Chen, X. Yao, and F. Zhu, Phys. Chem. Chem. Phys. **20**, 6606 (2018).

[46] L. Wang, Y. Wang, H. Sun, J. Zhao, and Q. Wang, Chem. Phys. Lett. **736**, 136785 (2019).

[47] G. Hu, A. Ma, and J. Wang, J. Chem. Inf. Model. **57**, 918 (2017).

[48] L. Duan, X. Liu, and J. Z. H. Zhang, J. Am. Chem. Soc. **138**, 5722 (2016).

[49] X. Jia, M. Wang, Y. Shao, G. König, B. R. Brooks, J. Z. H. Zhang, and Y. Mei, J. Chem. Theory Comput. **12**, 499 (2016).

[50] M. Aldeghi, A. Heifetz, M. J. Bodkin, S. Knapp, and P. C. Biggin, Chem. Sci. **7**, 207 (2016).

[51] Y. Gao, T. Zhu, and J. Chen, Chem. Phys. Lett. **706**, 400 (2018).

[52] L. F. Wang, Y. Wang, Z. Y. Yang, J. Zhao, H. B. Sun, and S. L. Wu, SAR QSAR Environ. Res. **31**, 373 (2020).

[53] W. Wang and A. Kollman Peter, Proc. Natl. Acad. Sci. USA **98**, 14937 (2001).

[54] T. Hou, J. Wang, Y. Li, and W. Wang, J. Comput. Chem. **32**, 866 (2011).

[55] Z. Sun, Z. Huai, Q. He, and Z. Liu, J. Chem. Inf. Model. **61**, 6107 (2021).

[56] W. Xue, F. Yang, P. Wang, G. Zheng, Y. Chen, X. Yao, and F. Zhu, ACS Chem. Neurosci. **9**, 1128 (2018).

[57] T. Hou and R. Yu, J. Med. Chem. **50**, 1177 (2007).

[58] J. Su, X. Liu, S. Zhang, F. Yan, Q. Zhang, and J. Chen, Chem. Biol. Drug Des. **93**, 163 (2019).

[59] D. Shi, Q. Bai, S. Zhou, X. Liu, H. Liu, and X. Yao, Proteins **86**, 43 (2018).

[60] M. Aldeghi, A. Heifetz, M. J. Bodkin, S. Knapp, and P. C. Biggin, J. Am. Chem. Soc. **139**, 946 (2017).

[61] M. Shi, J. He, T. Weng, N. Shi, W. Qi, Y. Guo, T. Chen, L. Chen, and D. Xu, Phys. Chem. Chem. Phys. **24**, 5125 (2022).

[62] Q. Wang, Y. Li, J. Xu, Y. Wang, E. L. H. Leung, L. Liu, and X. Yao, Sci. Rep. **7**, 8857 (2017).

[63] J. Chen, X. Liu, S. Zhang, J. Chen, H. Sun, L. Zhang, and Q. Zhang, Phys. Chem. Chem. Phys. **22**, 2262 (2020).

[64] P. Auffinger and E. Westhof, J. Mol. Biol. **269**, 326 (1997).

[65] L. S. D. Caves, J. D. Evanseck, and M. Karplus, Protein Sci. **7**, 649 (1998).

[66] B. Knapp, L. Ospina, and C. M. Deane, J. Chem. Theory Comput. **14**, 6127 (2018).

[67] J. Chen, J. Wang, B. Yin, L. Pang, W. Wang, and W. Zhu, ACS Chem. Neurosci. **10**, 4303 (2019).

[68] Y. Wang, S. Wu, L. Wang, Z. Yang, J. Zhao, and L. Zhang, RSC Adv. **11**, 745 (2021).

[69] J. chen, B. Yin, L. Pang, W. Wang, J. Z. H. Zhang, and T. Zhu, J. Biomol. Struct. Dyn. **38**, 2141 (2020).

[70] S. Liang, X. Liu, S. Zhang, M. Li, Q. Zhang, and J. Chen, Phys. Chem. Chem. Phys. **24**, 1743 (2022).

[71] J. Chen, S. Zhang, Q. Zeng, W. Wang, Q. Zhang, and X. Liu, Fron. Mol. Biosci. **9**, 912518 (2022).

[72] F. Yan, X. Liu, S. Zhang, J. Su, Q. Zhang, and J. Chen, Int. J. Mol. Sci. **19**, 2496 (2018).

[73] J. T. Seal, S. J. Atkinson, H. Aylott, P. Bamborough, C. W. Chung, R. C. B. Copley, L. Gordon, P. Grandi, J. R. J. Gray, L. A. Harrison, T. G. Hay-

DOI: 10.1063/1674-0068/cjcp2208126

how, M. Lindon, C. Messenger, A. M. Michon, D. Mitchell, A. Preston, R. K. Prinjha, I. Rioja, S. Taylor, I. D. Wall, R. J. Watson, J. M. Woolven, and E. H. Demont, J. Med. Chem. **63**, 9093 (2020).
[74] S. W. Ember, Q. T. Lambert, N. Berndt, S. Gunawan, M. Ayaz, M. Tauro, J. Y. Zhu, P. J. Cranfill, P. Greninger, C. C. Lynch, C. H. Benes, H. R. Lawrence, G. W. Reuther, N. J. Lawrence, and E. Schönbrunn, Mol. Cancer Ther. **16**, 1054 (2017).
[75] T. Ichiye and M. Karplus, Proteins **11**, 205 (1991).
[76] J. Chen, L. Wang, W. Wang, H. Sun, L. Pang, and H. Bao, Comput. Biol. Med. **135**, 104639 (2021).
[77] R. M. Levy, A. R. Srinivasan, W. K. Olson, and J. A. McCammon, Biopolymers **23**, 1099 (1984).
[78] A. E. García, Phys. Rev. Lett. **68**, 2696 (1992).
[79] R. M. Karim, M. J. Bikowitz, A. Chan, J. Y. Zhu, D. Grassie, A. Becker, N. Berndt, S. Gunawan, N. J. Lawrence, and E. Schönbrunn, J. Med. Chem. **64**, 15772 (2021).
[80] R. Anandakrishnan, B. Aguilar, and A. V. Onufriev, Nucleic Acids Res. **40**, W537 (2012).
[81] A. Jakalian, B. L. Bush, D. B. Jack, and C. I. Bayly, J. Comput. Chem. **21**, 132 (2000).
[82] A. Jakalian, D. B. Jack, and C. I. Bayly, J. Comput. Chem. **23**, 1623 (2002).
[83] J. Wang, R. M. Wolf, J. W. Caldwell, P. A. Kollman, and D. A. Case, J. Comput. Chem. **25**, 1157 (2004).
[84] J. P. Ryckaert, G. Ciccotti, and H. J. C. Berendsen, J. Comput. Phys. **23**, 327 (1977).
[85] W. L. Jorgensen, J. Chandrasekhar, J. D. Madura, R. W. Impey, and M. L. Klein, J. Chem. Phys. **79**, 926 (1983).
[86] T. Darden, D. York, and L. Pedersen, J. Chem. Phys. **98**, 10089 (1993).
[87] U. Essmann, L. Perera, M. L. Berkowitz, T. Darden, H. Lee, and L. G. Pedersen, J. Chem. Phys. **103**, 8577 (1995).
[88] S. Le Grand, A. W. Götz, and R. C. Walker, Comput. Phys. Commun. **184**, 374 (2013).
[89] A. W. Götz, M. J. Williamson, D. Xu, D. Poole, S. Le Grand, and R. C. Walker, J. Chem. Theory Comput. **8**, 1542 (2012).
[90] R. Salomon Ferrer, A. W. Götz, D. Poole, S. Le Grand, and R. C. Walker, J. Chem. Theory Comput. **9**, 3878 (2013).
[91] J. Wang, P. Morin, W. Wang, and P. A. Kollman, J. Am. Chem. Soc. **123**, 5221 (2001).
[92] J. Su, X. Liu, S. Zhang, F. Yan, Q. Zhang, and J. Chen, Chem. Biol. Drug Des. **91**, 828 (2018).
[93] J. Chen, S. Zhang, W. Wang, H. Sun, Q. Zhang, and X. Liu, ACS Chem. Neurosci. **12**, 2591 (2021).
[94] E. L. Wu, K. Han, and J. Z. H. Zhang, Chem. Eur. J. **14**, 8704 (2008).
[95] H. Sun, Y. Li, S. Tian, L. Xu, and T. Hou, Phys. Chem. Chem. Phys. **16**, 16719 (2014).
[96] H. Sun, Y. Li, M. Shen, S. Tian, L. Xu, P. Pan, Y. Guan, and T. Hou, Phys. Chem. Chem. Phys. **16**, 22035 (2014).
[97] D. Sitkoff, K. A. Sharp, and B. Honig, J. Phys. Chem. **98**, 1978 (1994).
[98] H. Gohlke, C. Kiel, and D. A. Case, J. Mol. Biol. **330**, 891 (2003).
[99] B. R. Miller, T. D. McGee, J. M. Swails, N. Homeyer, H. Gohlke, and A. E. Roitberg, J. Chem. Theory Comput. **8**, 3314 (2012).
[100] B. Xu, H. Shen, X. Zhu, and G. Li, J. Comput. Chem. **32**, 3188 (2011).
[101] J. Chen, S. Zhang, W. Wang, L. Pang, Q. Zhang, and X. Liu, J. Chem. Inf. Model. **61**, 1954 (2021).
[102] M. Laberge and T. Yonetani, Biophys. J. **94**, 2737 (2008).
[103] A. D. McLachlan, J. Mol. Biol. **128**, 49 (1979).

DOI: 10.1063/1674-0068/cjcp2208126